



The CAIRN method: Automated, reproducible calculation of catchment-averaged denudation rates from cosmogenic radionuclide concentrations

Simon Marius Mudd¹, Marie-Alice Harel¹, Martin D. Hurst², Stuart W. D. Grieve¹, and Shasta M. Marrero¹

¹School of GeoSciences, University of Edinburgh, Drummond Street, Edinburgh EH8 9XP, UK

²British Geological Survey, Keyworth, Nottingham NG12 5GG, UK

Correspondence to: Simon M. Mudd (simon.m.mudd@ed.ac.uk)

Abstract. The use of cosmogenic radionuclides to calculate catchment-averaged denudation rates has become a widely adopted technique in the last two decades, yet the methodology varies between studies and is not always reproducible. We report a new program for calculating catchment-averaged denudation rates from cosmogenic radionuclide concentrations. The method (Catchment-Averaged denudation Rates from cosmogenic Nuclides: CAIRN) bundles previously reported production scaling and topographic shielding algorithms. In addition, it calculates production and shielding on a pixel-by-pixel basis. We explore the sampling frequency across both azimuth ($\Delta\theta$) and altitude ($\Delta\phi$) angles for topographic shielding and show that in high relief terrain a relatively high sampling frequency is required, with a good balance achieved between accuracy and computational expense at $\Delta\theta = 8^\circ$ and $\Delta\phi = 5^\circ$. The method includes both internal and external uncertainty analysis, and is packaged in freely available software in order to facilitate easily reproducible denudation rate estimates. CAIRN calculates denudation rates but also automates catchment averaging of shielding and production, and thus can be used to provide reproducible input parameters for the CRONUS family of online calculators.

1 Introduction

In-situ cosmogenic radionuclides (CRNs), such as ¹⁰Be and ²⁶Al, are widely used to determine both exposure ages and denudation rates (e.g., Dunai, 2010; Granger et al., 2013; von Blanckenburg and Willenbring, 2014; Granger and Schaller, 2014). A denudation rate is the sum of the chemical weathering rate and physical erosion rate. Since the publication of the seminal papers by Brown et al. (1995), Granger et al. (1996) and Bierman and Steig (1996), dozens of studies have used concen-



trations of CRNs in stream sediments to quantify denudation rates that are spatially averaged over eroding drainage basins. There are now more than 1000 published catchment-averaged denudation rates (e.g., Portenga and Bierman, 2011; Willenbring et al., 2013a), with many new studies published each year.

25 Several authors have provided standardized methods for calculating denudation rates from CRN concentrations, notably the COSMOCALC package (Vermeesch, 2007) and the CRONUS-Earth online calculator (Balco et al., 2008). Here we make comparisons with the CRONUS calculator version 2.2, so we refer to it as CRONUS-2.2 for clarity. These calculators have been widely adopted by the cosmogenic, quaternary science and geomorphic communities, in large part because they are easily accessible and their methods are transparent (i.e., the source files are available online). These previously published cosmogenic calculators are ideal for calculating denudation rates or ages from a particular site (e.g., an exposed surface or a glacial moraine). However, using these calculators to determine catchment-averaged denudation rates necessitates the user selecting representative parameters for the catchment and an open-source method of making these choices has yet to emerge. Due to the lack of an open-source tool, a wide variety of approaches to calculating catchment-averaged denudation rates are used in the literature, which makes intercomparison studies challenging (c.f., Portenga and Bierman, 2011; Willenbring et al., 2013a).

Several factors determine the concentration of a CRN in a sample. For instance, elevation and latitude control the production rate of different CRNs (e.g., Lal, 1991; Dunai, 2000; Stone, 2000; Desilets and Zreda, 2003; Lifton et al., 2005). Production rates vary within a basin and thus users of online calculators frequently choose values ‘representative’ of the entire catchment. As such, online calculators ingest single parameters representative of an entire catchment for production rates and scaling factors, either in combination (COSMOCALC) or separately (CRONUS-2.2). For example, many authors use an averaging scheme for production where production is calculated in each pixel, and a representative value is then passed to an online calculator (e.g., Kirchner et al., 2001; Hurst et al., 2012; Munack et al., 2014; Scherler et al., 2014). In addition, CRN concentrations can be affected by partial shielding caused by snow cover, surrounding topography, and overlying layers of sediment (e.g., Balco et al., 2008). These again are spatially distributed and so authors reporting catchment-averaged denudation rates frequently report averaged shielding values. Although software packages do exist for calculating spatially averaged topographic shielding (e.g., Codilean, 2006) and snow shielding (e.g., Schildgen et al., 2005), results from these models are not integrated with spatially varying production rates. Finally, in landslide dominated terrain, removal of thick layers of sediment can dilute CRN concentrations in river sediment (Niemi et al., 2005; Yanites et al., 2009; West et al., 2014). This factor is often not included in denudation calculations. For these reasons, Balco et al. (2008) specifically urged development of tools dedicated to the calculation of catchment-averaged denudation rates from CRN concentrations.



Here we present software that estimates production and shielding of the CRNs ^{10}Be and ^{26}Al on a pixel-by-pixel basis, and propagates uncertainty in AMS measurement and CRN production. We have made this software available through an open-source platform at [https://github.com/LSDtopotools/](https://github.com/LSDtopotools/LSDTopoTools_CRNBasinwide)
60 LSDTopoTools_CRNBasinwide to allow community modification and scrutiny, with the goal of allowing users to report denudation rates that can be easily reproduced by other scientists.

2 Solution of CRN concentration at a single location

We derive a solution that tracks the concentration of a CRN as it is exposed, exhumed or buried. This approach is adopted because we feel it is the most general: specific scenarios of both steady
65 and transient denudation and burial may therefore be derived. Our approach is broadly similar to that of Parker and Perg (2005), but results are equivalent to those of more widely used derivations (e.g., Lal, 1991; Granger and Smith, 2000).

We begin by conserving the concentration of CRN i through time t :

$$\frac{dC_i}{dt} = P_i - \lambda_i C_i \quad (1)$$

70 where C_i is the concentration of CRN i (C_i is typically reported in atoms g^{-1} , i could be ^{10}Be or ^{26}Al , for example), P_i is the production rate of CRN i (in atoms $\text{g}^{-1} \text{yr}^{-1}$) and λ_i (yr^{-1}) is the decay constant of CRN i . Production can be a function of latitude, altitude (or atmospheric pressure), magnetic field strength and shielding by rock, soil, water or snow (e.g., Balco et al., 2008).

CRNs can be produced by both neutrons and muons (e.g., Gosse and Phillips, 2001). Production
75 by neutrons is widely modelled using a simple function in which production decays exponentially with depth (e.g., Lal, 1991). Muons, on the other hand, are modelled using a variety of schemes. The CRONUS-2.2 calculator (Balco et al., 2008) implements the scheme of Heisinger et al. (2002a, b), which requires computationally expensive integration of muon stopping over a depth profile. Recent field-based estimates of muon production suggest that Heisinger et al. significantly overestimates
80 production by muons (Braucher et al., 2011, 2013; Phillips et al., 2016a). For both computational efficiency and flexibility in selecting muon production scaling terms, we use a model similar to those used by Granger and Smith (2000), Braucher et al. (2009), Schaller et al. (2009), and Vermeesch (2007) where the production rate is the sum of four exponential functions:

$$P_i(d) = P_{i,SLHL} \sum_{j=0}^3 S_{i,j} F_{i,j} e^{-\frac{d}{\lambda_j}} \quad (2)$$

85 where $P_{i,SLHL}$ is the surface production rate (atoms $\text{g}^{-1} \text{yr}^{-1}$) at sea level and high latitude, $F_{i,j}$ is a dimensionless scaling that relates the relative production of neutron spallation and muon production, $S_{i,j}$ is a dimensionless scaling factor that lumps the effects of production scaling and shielding of



cosmic rays, d is a mass per unit area which represents the mass overlying a point under the surface
 (g cm^{-2} typically), and Λ_j is the attenuation length for reaction type j (g cm^{-2}). The reaction types
 90 are $j = 0$ for neutrons and $j = 1 - 3$ for muons; these can be either slow or fast muons.

The depth d , called shielding depth, is related to depth below the surface as:

$$d = \int_{\zeta-h}^{\zeta} \rho(z) dz \quad (3)$$

where ζ (cm) is the elevation of the surface, h (cm) is the depth in the subsurface of the sample, z
 (cm) is the elevation in a fixed reference frame and ρ (g cm^{-3}) is the material density, which may be
 95 a function of depth. For a constant density, $d = \rho h$.

2.1 Solving the governing equation

The governing equation (Eq. 1) has the general form:

$$\frac{dC}{dt} + p(t)C = g(t) \quad (4)$$

In our case, $p(t)$ simply equals λ_i , which is a constant in this case, and $g(t)$ is equal to P_i , which is
 100 a function of t .

Equations of this form have the solution:

$$C = \frac{1}{h(t)} \int h(t)g(t) dt + const \quad (5)$$

where $const$ is an integration constant and

$$h(t) = \exp\left(\int p(t) dt\right) \quad (6)$$

105 which in the case of the cosmogenic governing equation reduces to:

$$h(t) = e^{\lambda_i t} \quad (7)$$

The term $g(t)$ is equal to:

$$g(t) = P_{i,SLHL} \sum_{j=0}^3 S_{i,j} F_{i,j} e^{-\frac{d}{\Lambda_j}} \quad (8)$$

The shielding depth d is a function of time:

$$110 \quad d(t) = d_0 + \int_{t_0}^t \epsilon(\tau) d\tau \quad (9)$$



where τ is a dummy variable for time that is replaced by the limits after integration. In the case where denudation, denoted ϵ ($\text{g cm}^{-2} \text{ yr}^{-1}$), is steady in time this becomes

$$d(t) = d_0 + \epsilon(t_0 - t) \quad (10)$$

where t_0 is the initial time. Here denudation is the rate of removal of mass from above the sample per unit area. If we let the concentration of the CRN equal C_0 at the initial time t_0 and combine Eqs. (5), (7), (8), and (10), we can solve for the integration constant (*const*) and arrive at a solution for CRN i at time t :

$$C_i(t) = C_0 e^{-(t-t_0)\lambda_i} + P_{i,SLHL} \left[\sum_{j=0}^3 \frac{S_{i,j} F_{i,j} \Lambda_{i,j}}{\epsilon + \Lambda_{i,j} \lambda} e^{\frac{-d_0}{\Lambda_{i,j}}} \left(e^{\frac{\epsilon(t-t_0)}{\Lambda_{i,j}}} - e^{-(t-t_0)\lambda} \right) \right] \quad (11)$$

Equation (11) is the full governing equation from which scenario-specific solutions may be derived.

120 2.2 Steady state solution

By convention, we consider the cosmogenic profile to be steady in time. This allows analytical solution of the CRN concentration at any point in the basin. At steady state, the particles near the surface have been removed (either through erosion or chemical weathering) at the same rate for a very long time, so we set $t_0 = 0$ and $t = \infty$. This results in a simplified form:

$$125 \quad C_i(d) = P_{i,SLHL} \sum_{j=0}^3 \frac{S_{i,j} F_{i,j} \Lambda_{i,j} e^{-d/\Lambda}}{\epsilon + \lambda_i \Lambda_{i,j}} \quad (12)$$

where ϵ is the denudation rate ($\text{g cm}^{-2} \text{ yr}^{-1}$). If we set $d = 0$ (that is, we solve for material being eroded from the surface, with no distributed mass loss via weathering), Eq. (12) reduces to Eq. (6) from Granger and Smith (2000) for denudation only (i.e., no burial or exposure), and reduces to Eq. (8) of Lal (1991) if production is due exclusively to neutrons.

130 2.3 Snow and self-shielding

Equation (12) is restrictive in that it only considers material removed from a specific depth, i.e. removed for a single value of d . In reality samples may come from a zone of finite thickness. This finite thickness can contribute some shielding to the sample, i.e. the bottom of a sample is shielded by the mass of the sample that overlies. This shielding is called self-shielding and is generally implemented by assuming that self-shielding can simply be approximated by a reduction in neutron production (e.g., Vermeesch, 2007; Balco et al., 2008). Snow can also reduce production of CRNs (e.g., Gosse and Phillips, 2001). Typically these two forms of shielding (snow and self) are typically incorporated in denudation rate calculators as a scaling coefficient calculated before solution of the



governing equations (e.g., Vermeesch, 2007; Balco et al., 2008), i.e. snow and self-shielding are
140 incorporated into the $S_{i,j}$ term.

Our strategy is slightly different: we calculate snow and self-shielding by integrating the CRN
concentration over a finite depth in eroded material. For example, if there is no snow, the concen-
tration of CRNs at a given location is obtained by depth-averaging the steady concentrations from
zero depth (the surface) to the thickness of eroded material. If snow is present, the concentration
145 is determined by depth-averaging from the mean snow depth (d_s) to the thickness of the removed
material (d_t). Both d_s and d_t are shielding thicknesses, therefore they are in units of g cm^{-2} and thus
differences in material density are taken into account. The depth-averaged concentration is then:

$$C_i(d) = \frac{P_{i,SLHL}}{d_t} \sum_{j=0}^3 \frac{S_{i,j} F_{i,j} \Lambda_{i,j}^2 (e^{-d_s/\Lambda_{i,j}} - e^{-(d_s+d_t)/\Lambda_{i,j}})}{\epsilon + \lambda_i \Lambda_{i,j}} \quad (13)$$

This approach also allows the computation of CRN concentration dilution due to landslides by
150 setting the thickness of removed material to the landslide thickness. Thicknesses can either be mea-
sured in the field, modelled (e.g., Niemi et al., 2005; Yanites et al., 2009), or approximated using
mapped landslide inventories (e.g., Hovius et al., 1997; Korup, 2005). These may be combined with
data on landslide area-volume relationships (e.g., Guzzetti et al., 2009). Our formulation (Eq. 13)
is still a steady state approximation in that it is assumed that material exhumed by landslides has a
155 concentration profile obtained from a single constant denudation rate, similar to Niemi et al. (2005).
We do not explore landsliding further as it is beyond the scope of this contribution, but simply note
here that our depth averaged approach allows calculation of dilution due to mass wasting.

2.4 Topographic shielding

In addition to snow and self-shielding, locations in hilly or mountainous areas can also receive a
160 reduced flux of cosmic rays because these have been shielded by surrounding topography (Dunne
et al., 1999). We adopt the method of Codilean (2006), in which both the effect of dipping sample
surfaces and shielding by topography blocking incoming cosmic rays are computed. The Codilean
(2006) method is spatially distributed: each pixel in a digital elevation model (DEM) has its own to-
pographic shielding correction that varies from 0 (completely shielded) to 1 (no topographic shield-
165 ing). These correction values are calculated by modelling shadows cast upon each pixel in the DEM
from every point in the sky. This is achieved by modelling shadows incrementally for a range of
zenith (ϕ) values from 0° to 90° and azimuth (θ) values from 0° to 360° .

As $\Delta\theta$ and $\Delta\phi$ values decrease, the accuracy with which the shielding is calculated is expected
to increase, as we are modelling shielding at finer resolutions. However, this benefit is attenuated by
170 increasing computational cost when these values tend towards (1° , 1°). Codilean (2006) compared
the accuracy of different $\Delta\theta$ and $\Delta\phi$ by comparing them to a minimum step size of (5° , 5°). Here we
exploit the efficiency of our software and the considerable increase in computing power since 2006



to explore smaller step sizes. We make the assumption that a step size of (1° , 1°), corresponding to 32400 iterations of the shielding algorithm, is an accurate representation of the true shielding factor
175 to the extent that any further refinement in the measurements would not yield a significant change in the results of the CRN calculations.

In order to determine the optimal balance between measurement accuracy and computational efficiency, the full range of ($\Delta\theta$, $\Delta\phi$) pairs were used to derive shielding values for each cell of a worst-case scenario: a high-relief section of the Himalaya (650 km^2 with a 7000 m range in elevation). Table 1 presents the maximum absolute residual value (the error of the pixel with the greatest
180 error) for topographic shielding of the corresponding step sizes when compared to the shielding derived for (1° , 1°). Using values below Codilean (2006)'s suggested threshold of (5° , 5°) gives increasingly small returns for a larger computational burden. We suggest that a ($\Delta\theta$, $\Delta\phi$) pair of (8° , 5°), requiring 810 iterations, is an optimal value for any high relief landscape, yielding a maximum
185 absolute error in our test site of 0.018. On lower relief landscapes the ($\Delta\theta$, $\Delta\phi$) values could be increased to achieve the same level of accuracy. We note that these data are determined using a 90 m resolution DEM, and errors will be higher for finer resolution DEMs (Norton and Vanacker, 2009).

2.5 Production scaling

Production of CRNs varies as a function of both elevation (defined via atmospheric pressure) and
190 latitude and these variations are accounted for by using one of several possible scaling schemes. The classic scaling model of Lal (1991), later modified by Stone (2000), is the simplest and is referred to herein as Lal/Stone. Later scaling models (Dunai, 2000, 2001; Desilets and Zreda, 2003; Lifton et al., 2005, 2014) have incorporated various other parameters such as time-dependent geomagnetic field variations, solar modulation, and nuclide-specific information, resulting in a total of seven possible
195 scaling models in the most recent CRONUS calculator (Marrero et al., 2016).

These scaling schemes vary in complexity and therefore computational expense. Time-dependent scaling schemes are far more computationally expensive than the time-independent scheme of Lal/Stone, which does not consider variations in geomagnetic field strength. Recent calibration results (Borchers et al., 2016; Phillips et al., 2016a), including a low-latitude, high-altitude site in Peru (Kelly et al.,
200 2015; Phillips et al., 2016b) suggest that the time-independent Lal/Stone scheme performs similarly to the physics-based schemes presented in Lifton et al. (2014) and fits the data better than several other scaling schemes (Dunai, 2000; Desilets and Zreda, 2003; Lifton et al., 2005). For these reasons, we scale production rates using the Lal/Stone scheme.

The Lal/Stone scaling scheme requires air pressure, whereas most published studies include only
205 elevation information. We follow the approach of Balco et al. (2008) and convert latitude and elevation data to pressure using the NCEP2 climate reanalysis data (Compo et al., 2011). In certain areas, the ERA-40 reanalysis (Uppala et al., 2005) has been shown to provide more accurate results and due to CAIRN's open source design new models can be readily incorporated into the software. Here



we retain the NCEP2 reanalysis to better compare our results with CRONUS-2.2. We note that if
210 users deploy CAIRN as a spatial averaging front end to online calculators, they should be vigilant to
use the same air pressure conversion method in both CAIRN and the online calculator.

2.6 Combining scaling and shielding

To calculate the concentration of a CRN, the scaling factors for each pathway ($S_{i,j}$) must be com-
puted. Both topographic shielding and production rate scaling are subsumed within the scaling
215 terms ($S_{i,j}$), whereas snow and self-shielding are computed separately (see Sect. 2.3). We follow
the method of Vermeesch (2007) and calculate scaling factors using an effective attenuation depth.
We must do this because, when considering multiple production pathways, the scaling terms for
individual production mechanisms may vary depending on elevation, shielding, sample thickness,
or denudation rates. For example, muogenic pathways will contribute relatively more to production
220 when there is more shielding since muogenic reactions penetrate deeper than spallation.

To determine the scaling terms for the individual production mechanisms ($S_{i,j}$), we first compute
the total scaling at a location (S_{tot}), which we define as the product of the production rate scaling
(S_p) and the topographic shielding (S_t), that is $S_{tot} = S_t S_p$. Production scaling (S_p) is estimated us-
ing the Lal/Stone scaling scheme and (S_t) is calculated using our topographic shielding algorithms.
225 We then derive the scaling factors for the individual production mechanisms, $S_{i,j}$, by employing a
virtual attenuation length, Λ_v , in units of g cm^{-2} , following the method of Vermeesch (2007):

$$S_{i,j} = e^{-\frac{\Lambda_v}{\Lambda_i}} \quad (14)$$

We must therefore calculate Λ_v based on S_{tot} . The individual production mechanisms must be set
such that:

$$230 \quad S_{tot} = \sum_{j=0}^3 S_{i,j} F_{i,j} \quad (15)$$

In Eq. (15), S_{tot} and $F_{i,j}$ are known, whereas $S_{i,j}$ are functions of Λ_v . We thus iterate upon Λ_v ,
calculating $S_{i,j}$ using Eq. (14) using Newton's method until Eq. (15) converges on a solution for Λ_v .
Once the virtual attenuation length is solved, the $S_{i,j}$ terms are then used in Eq. (13).

3 Denudation rates across a catchment

235 So far we have described the calculations that predict the concentration of a CRN at one specific
location in a basin. Some form of this method is embedded within existing CRN calculators. A wide
variety of approaches to scale calculations of CRN concentrations within a single location to the
concentration across entire catchments have been used in the literature. Some authors have aver-
aged production rates on a pixel-by-pixel basis but have not considered topographic shielding (e.g.,



240 Belmont et al., 2007; DiBiase et al., 2010; Portenga and Bierman, 2011). Others have calculated an average scaling by integrating the product of topographic shielding and production on a pixel-by-pixel basis (e.g., Ouimet et al., 2009; Hurst et al., 2012; Lupker et al., 2012; Scherler et al., 2014). Another strategy is to calculate both averaged topographic shielding and production scaling values for a basin (e.g., Abbühl et al., 2010). All of these approaches involve some degree of spatial averaging of production, shielding, or a combination of the two before catchment-averaged denudation rates are estimated.

The approach we take in the CAIRN method differs in that shielding and production rates are not averaged: these are calculated locally at each pixel. For a given denudation rate ϵ , the concentration of CRNs from each pixel is calculated, then the catchment-averaged concentration is the average of the concentrations from all pixels. In applications without landsliding, this concentration requires no weighting because the denudation rate is considered to be spatially homogenous. In the event of mass removal (i.e., by setting d_t in Eq. 13), the average concentration is weighted by the local thickness of mass removed to account for increased volumes derived from material delivered to the basin through mass wasting. The denudation rate for the basin is then iterated upon with Newton's method until the predicted concentration of CRNs emerging from the catchment matches the measured concentration (see Algorithm 1).

We should note here that the version of CAIRN reported in this contribution calculates the denudation rate across an entire catchment required to produce the observed concentration of the target CRN. That is, CAIRN assumes denudation rates are the same everywhere in the catchment. Even in the case of removal of spatially heterogeneous mass of known thickness from the surface (i.e., by setting d_t Eq. 13), CAIRN still calculates the spatially homogenous background denudation rate in light of dilution by mass wasting or stripping of material from the landscape. Future adaptations of the (open source) code could account for nested basins (this sampling strategy common in many studies of basin averaged erosion rates) or changes in the concentration of target minerals (usually quartz) as employed by, for example Safran et al. (2006). These potential future developments, however, are beyond the scope of this contribution.

4 Uncertainty propagation

We calculate uncertainty from both internal (nuclide concentration uncertainties from accelerator mass spectrometry (AMS) measurements) and external (shielding and production rate) sources using Gaussian error propagation following Balco et al. (2008). We do note that some authors have used a Monte Carlo approach in determining CRN-derived denudation rates because parameter uncertainties can have non-gaussian distributions (e.g., West et al., 2015). CAIRN, at present, does not implement a Monte Carlo uncertainty approach but rather follows conventional Gaussian error propagation.



275 4.1 Gaussian error propagation

Uncertainties are calculated in terms of the denudation rate, ϵ , in units of $\text{g cm}^{-2} \text{ yr}^{-1}$, so that no assumption about bedrock density is necessary. The standard deviation of the denudation rate, s_ϵ , is calculated with

$$s_\epsilon = \sqrt{\left(\frac{\partial \epsilon}{\partial x}\right)^2 s_x^2 + \left(\frac{\partial \epsilon}{\partial y}\right)^2 s_y^2 + \dots} \quad (16)$$

280 where s_x is the standard deviation of x , s_y is the standard deviation of y , and so on. The variables x and y can represent any uncertain parameter, such as the measurement uncertainty or the production rate of the nuclide. All uncertainties (e.g., nuclide concentration) are assumed to be at the one sigma level unless otherwise stated. The derivatives in Eq. (16) are calculated using the nominal value plus the associated uncertainty and then recalculating the denudation rate in the original, pixel-by-pixel
285 fashion.

Three uncertainties are included in the calculation: i) the uncertainty in CRN concentration, ii) the uncertainty in the production rate at sea level, high latitude ($P_{i,SLHL}$), and iii) uncertainty in muon production. Uncertainty in CRN concentration is reported by authors alongside concentrations. For the CRN concentration uncertainty, the concentration is used directly to determine the denudation
290 rate uncertainty. For all other parameters, the uncertainty values help to predict a new concentration in each pixel, which is then used to determine denudation rate uncertainty.

The uncertainty on the production rate ($P_{i,SLHL}$) is the same as that used in the CRONUS-2.2 calculator (Balco et al., 2008): $0.39 \text{ atoms cm}^{-2} \text{ yr}^{-1}$ for ^{10}Be and $2.63 \text{ atoms cm}^{-2} \text{ yr}^{-1}$ for ^{26}Al (based on a ratio of production between ^{26}Al and ^{10}Be of 6.1×1.106). Although the recent CRONUS-Earth
295 calibration (Borchers et al., 2016) has produced new production rates for both ^{10}Be and ^{26}Al , the production rate uncertainties remain in the same range as those used here (Phillips et al., 2016a).

Even though recent studies seem to agree that muon production based on laboratory experiments (Heisinger et al., 2002a, b) overestimate muon production observed in deep samples (Braucher et al., 2003, 2011, 2013; Balco et al., 2013; Phillips et al., 2016a), there is still some uncertainty over the
300 exact muon production profile. CAIRN employs the exponential scaling method from Braucher et al. (2009). However, we use a very conservative estimate of uncertainty by calculating the contribution of muon models to overall uncertainty based on the difference between the default CAIRN muon model and those from the Schaller et al. (2009) scheme, which approximates the original Heisinger results (Heisinger et al., 2002a, b).

305 4.2 Uncertainty from snow and self-shielding (including landsliding)

Uncertainties from nuclide concentration, muon production, and production rates are calculated internally by our software. Uncertainties from snow and self-shielding rely on user-supplied information and therefore must be estimated separately.



Snow shielding can be supplied as a constant effective snow thickness (in g cm^{-2}) or spatially distributed information in the form of a raster. Most snow shielding calculations reported in the literature are based on an effective attenuation estimated by the thickness of snow (e.g. Balco et al., 2008), but recent field-based measurement indicate that snow may attenuate fluxes of cosmic rays to a greater extent than assumed in simple mass-based snow shielding calculations (Zweck et al., 2013; Delunel et al., 2014). However these uncertainties are small compared to the extreme uncertainties of the thickness, extent and duration of snow over millennial timescales, which are unlikely to ever be well constrained. If no snow shielding values are provided, the software assumes that there is no snow cover.

Similarly, self-shielding thickness can be supplied as a single value (in g cm^{-2}) or as spatially distributed thicknesses. For landsliding, the assumption is that there is a steady background denudation rate and then material with a steady cosmogenic depth profile is removed suddenly, which is the approach taken by Niemi et al. (2005). We do not account for re-equilibration of cosmogenic concentration that takes place in the years after a landslide (e.g., Schaller and Ehlers, 2006; Muzikar, 2009; Yanites et al., 2009). This would require a model or reconstruction of past landslides, which is beyond the scope of this contribution. Our landsliding module is admittedly rudimentary and is provided primarily as a tool for exploration. It allows users to calculate a spatially homogenous background denudation rate given a spatially distributed episode of instantaneous mass removal. This is obviously a contrived scenario but does allow users to probe whether the dilution by landslides of different sizes is likely to alter the inferred denudation rate within a catchment.

To calculate uncertainties, users must supply two scenarios for these shielding factors. For example, the user could provide two snow thickness rasters representing variation in snow thickness with 1σ uncertainty (how an author might calculate this could fill another paper and is beyond the scope of our study). The denudation rates of these two scenarios would then be calculated, and the square of the difference in these two denudation rates would then be inserted into Eq. (16). In this way users can calculate shielding uncertainties manually.

4.3 Summary of CAIRN parameters for denudation calculations

To summarize, the CAIRN method predicts CRN production from neutrons and muons using a four exponential approximation of data from Braucher et al. (2009). These production rates are scaled using Lal/Stone time-independent scaling. Production is calculated at every pixel, with atmospheric pressure calculated via interpolation from the NCEP2 reanalysis data (Compo et al., 2011). Topographic shielding is calculated using the method of Codilean (2006), and scaled production rates are multiplied by topographic, snow, and self-shielding at each pixel. Decay rates, attenuation lengths, and parameters for production are reported in Table 3. The CAIRN software prints these parameters to a file so that if they change in the future based on new calibration datasets, users will be able to both view and report these updated values.



345 5 Spatial averaging for ingestion by other denudation rate calculators

In addition to producing denudation rates, CAIRN also provides spatially-averaged production rates and effective catchment-averaged pressure (see below), so that users can compute denudation rates using other available calculators. Programs such as the CRONUS-Earth calculators (referred to as CRONUS-2.2 for Balco et al. (2008) and CRONUScalc for Marrero et al. (2016)) and COSMO-
350 CALC do not have the ability to calculate catchment-averaged parameters. CAIRN can be used independently to determine production rates or in conjunction with these other calculators, which allows for the possibility of using time-dependent scaling and other new features in the future.

The calculators require slightly different input parameters than those used directly in CAIRN. Because our depth-integrated treatment of cosmogenic concentrations (i.e., Eq. 13) differs from that
355 of COSMOCALC and the CRONUS calculators, we calculate snow and self-shielding using more traditional shielding terms for spatial averaging for use in these calculators.

Self-shielding used for spatial averaging is calculated for each pixel k with:

$$S_{self,k} = \frac{\Lambda_{i,0}}{d_{t,k}} \left(1 - e^{-\frac{d_{t,k}}{\Lambda_{i,0}}} \right) \quad (17)$$

where $S_{self,k}$ is the self-shielding correction for the k^{th} pixel, $d_{t,k}$ is the shielding thickness for the
360 k^{th} pixel (in g cm^{-2}). Equation (17) is used in both COSMOCALC and CRONUS. In the CRONUS calculators, snow shielding is lumped with topographic shielding, therefore the CRONUS calculators presumes the user will determine the product of snow and topographic shielding at a site with a method of their choice. COSMOCALC includes a snow shielding calculator which assumes that the equivalent depth of snow (in g cm^{-2}) attenuates neutron production following the formula:

$$365 S_{snow,k} = e^{-\frac{d_{s,k}}{\Lambda_{i,0}}} \quad (18)$$

where $S_{snow,k}$ is the snow shielding correction of the k^{th} pixel and $d_{s,k}$ is the time-averaged depth of snow water equivalent in g cm^{-2} . We adopt this approximation when performing spatial averaging. Although recent work suggests snow may attenuate spallation to a greater degree than predicted by Eq. (18) (Delunel et al., 2014), the uncertainty in historic snow thickness will outweigh uncertainties
370 from the snow shielding equation. We therefore recommend that users include a large range of snow thickness in their uncertainty analysis, guided by historical observations of snow depth.



5.1 Spatial averaging for COSMOCALC

In COSMOCALC's erosion calculator (which calculates denudation), the required inputs are a combined shielding and scaling term, the CRN concentration and the uncertainty in the CRN concentration. We calculate the scaling factor S_{CCtot} , which is a lumped shielding and scaling term, with

$$S_{CCtot} = \frac{1}{N} \sum_{k=0}^N S_{snow,k} S_{topo,k} S_{self,k} S_{i,k} \quad (19)$$

where terms are calculated on a pixel-by-pixel basis. Snow shielding is calculated from Eq. (18), self-shielding is calculated from Eq. (17), and topographic shielding is calculated accounting for the effects of sloping samples and topography blocking cosmic rays (see Sect. 2.4). We wish to emphasize that CAIRN reports S_{CCtot} for users that wish to use it in COSMOCALC, whereas the denudation rates reported by CAIRN use Eq. 13 for snow and self shielding. Production scaling for CRN i at pixel k , $S_{i,k}$, is calculated using Eq. (15) and Lal/Stone scaling (Sect. 2.5).

5.2 Spatial averaging for the CRONUS calculators

The CRONUS calculators (CRONUS-2.2 and CRONUSCalc) require a lumped shielding value and information about either the elevation or pressure of the sample. Spatial averaging of the lumped shielding value, $S_{CRshield}$, is calculated with:

$$S_{CRshield} = \frac{1}{N} \sum_{k=0}^N S_{snow,k} S_{topo,k} S_{self,k} \quad (20)$$

Note that we fold the self-shielding into the lumped shielding term so that when transferring data to the CRONUS calculator the sample thickness should be set to 0. We also calculate an effective pressure by taking the average production rate over the basin:

$$S_{effp} = \frac{1}{N} \sum_{k=0}^N S_{i,k} \quad (21)$$

We then use the Newton iteration on the Lal/Stone scaling scheme to find the pressure which reproduces the basin average production rate (S_{effp}). That way, results from our method can be compared to results from the CRONUS calculator and, if users are so inclined, they can use time varying production scalings via the CRONUS calculator (which CAIRN does not include for reasons outlined in Sect. 2.5).

6 Method comparison

Comparison with other methods is difficult because authors reporting CRN-derived catchment-averaged denudation rates have not made their algorithms available as open-source tools. Our spatially-



400 averaged production scaling and shielding estimates are approximations of spatial averaging reported
by other authors. We compare our data to both published denudation rate estimates, and to estimates
of denudation rates generated by the CRONUS calculator given the spatial averaging described in
5.2. In our comparisons we use seven published cosmogenic datasets (Table 2). These datasets were
chosen to span a wide range of locations (i.e., differing latitudes and elevations) and denudation
405 rates. The parameters used by CAIRN for these comparisons are reported in Table 3.

It will perhaps aid the reader to explain how denudation rate estimates may vary between meth-
ods. Firstly, production rates are nonlinearly related to elevation, and thus spatial averaging of the
product of production scaling and shielding is not the same as the product of the spatial averages
of production scaling and shielding. In addition, previous studies and other calculators have chosen
410 different parameters for CRN production and shielding. For example, past publications have used a
wide variety of methods for estimating topographic shielding (e.g., see Table 2). Choices of spalla-
tion and muon production rates also affect the final denudation rate. Consider a measured nuclide
concentration that one uses to infer an denudation rate. If one assumes a high production rate (via
either muons or spallation), it means that for a given denudation rate the predicted nuclide concen-
415 tration is higher. Thus, for a given nuclide concentration, the inferred denudation rate is higher if the
assumed production rate is higher (see dashed lines in Figure 1). If the inferred shielding is higher,
then for a given denudation rate the production is lower, and the inferred denudation for a given
concentration will be lower.

6.1 Spatial averaging of production and shielding vs pixel-by-pixel calculations

420 First, we compare results of two methods using the exponential approximation of muon production
(Eq. 12), used in both COSMOCALC and the CAIRN calculator. The difference in calculating de-
nudation rates by iterating upon CRN concentration from all pixels in a basin (the CAIRN method)
and calculating it by using a spatial average of the production of scaling and production terms (Eq.
19) is virtually zero if snow and self-shielding are spatially homogenous (Figure 2). Thus we find
425 that combining all scaling and shielding terms in a single lumped term is adequate for calculating
denudation rates if computational power is limited.

Separating production rate scaling from shielding leads to slightly larger uncertainty (Figure 3),
but in terms of the total uncertainty this averaging also leads to small uncertainties (on the order of
1-2% compared to 10-20% from other sources of uncertainty). Many users will want to compare
430 rates determined by our software with the popular CRONUS calculators (Balco et al., 2008; Marrero
et al., 2016). The CRONUS calculators internally scale production rates while shielding is a user
input. Consequently, the uncertainties plotted in Figure 3 approximate the uncertainties that will
arise from the spatial averaging process that users must pass to the CRONUS calculators. Some users
may wish to calculate denudation rates using geomagnetic scaling schemes, which is not possible in



435 CAIRN, but CAIRN can be used as a front end to the CRONUS calculators via its spatial averaging capabilities with the confidence that this will only introduce relatively small errors.

6.2 Comparison with existing denudation rate estimates

Denudation rates reported in the literature from catchment-averaged CRN concentrations are calculated using a wide variety of methods. The term erosion rate is often substituted for denudation rate
440 although few studies attempt to account for chemical weathering (cf., Kirchner et al., 2001). Studies differ in their strategies for production rate scaling, topographic, snow, and self-shielding, and the manner in which spatial averaging is performed. In many cases there is insufficient detail reported that might enable other groups to reproduce reported denudation rates. A primary motivation of the CAIRN calculator is to provide an open-source means of computing denudation rates that may then
445 be reproduced by other groups. We have incorporated reported snow shielding from previous studies by inverting Eq. 18 for an annual average snow thickness and then distributing this thickness over the entire DEM. We acknowledge this is a poor representation of snow thickness but snow shielding rasters are rarely available and in most cases there is little reported snow shielding.

The diversity in methods for calculating denudation rates reported in the literature means that it is
450 difficult to compare denudation rates when they come from different studies. This problem has been highlighted by previous data intercomparison studies (Portenga and Bierman, 2011; Willenbring et al., 2013a). Estimated sea level, high latitude production rates under Lal/Stone scaling of ^{10}Be have changed significantly over the last 15 years as more calibration sites are reported. For example Stone (2000) reported a value of $5.1 \text{ atoms g}^{-1} \text{ yr}^{-1}$, whereas the current estimates are closer to 4.0
455 $\text{atoms g}^{-1} \text{ yr}^{-1}$ (Borchers et al., 2016; Phillips et al., 2016a). This difference alone can lead to up to 20% differences in derived denudation rates. In some cases, muons are not considered, whereas other studies use a variety of different muon production schemes (e.g., Table 2). Studies typically report erosion or denudation rates in dimensions of length per time, but this requires an assumption about rock density, which can vary and is sometimes not reported. Topographic shielding is occasionally
460 not considered (particularly in older studies). In some cases the horizon elevation is recorded from a limited number of directions (e.g., COSMOCALC includes a calculator using 8 directions), and in other instances the computational method of Codilean (2006) is used. Studies also cite Dunne et al. (1999) for shielding but this paper lists several methods for calculating shielding: the equations therein depend on the number and geometry of shielding objects and this information is seldom
465 reported. Even when the more robust method of Codilean is used, the spacing of azimuth and angle of elevation is often not reported.

Of our seven example datasets (Table 2), only 3 of the original authors reported topographic shielding factors. We calculated shielding using the CAIRN method with $\Delta\phi = 5^\circ$, $\Delta\theta = 8^\circ$ in these three high relief landscapes using a 90 meter resolution DEM. Our small values of $\Delta\phi$ and $\Delta\theta$
470 systematically resulted in calculated topographic shielding well above (up to 20% more shielding)



the shielding factors used in previous studies (Figure 4). At the time of its publication, the Codilean (2006) algorithm was severely limited by computational power. Codilean reported a computing time of 46 hours for $\Delta\phi = 5^\circ$ and $\Delta\theta = 5^\circ$ on a relatively small DEMs (15 km² at 10 m resolution). Authors using Dunne et al.'s algorithm have used a limited number of horizon measurements to calculate
475 shielding. For example in COSMOCALC (Vermeesch, 2007), users are expected to input horizon values at 45° intervals, which can lead to errors of 10-40% in high relief landscapes (Table 1). An example of the potential underestimates of topographic shielding is shown in Figure 5.

The denudation rates predicted by CAIRN are plotted against reported denudation rates in Figure 6. These data are scattered about the 1:1 line, but for most samples the CAIRN denudation rate
480 is lower than the reported denudation rate. Reasons for this vary for each study since the method used to calculate denudation rates vary in each example study, but one unifying factor is that CAIRN calculates topographic shielding at much higher resolution than virtually all previous studies and as a result topographic shielding in CAIRN is significantly higher (i.e. lower S_t values), resulting in lower denudation rate estimates (see Figure 1). Higher production rates used in previous studies
485 (Table 2) also lead to higher reported denudation rates than those calculated by CAIRN. One component of CAIRN that requires some caution is that the snapping of cosmogenic samples to channels is automated: if errors in the DEM place the main channel in the wrong location, or GPS coordinates of the sampling location contain large errors (common in older datasets), there is a chance the basin selected by CAIRN will not be the same as the sampled basin. This can result in large errors as
490 production rates vary significantly with elevation. We have provided a tool in the github repository that allows users to check the basins that are associated with CRN samples. If these do not match the expected basins, then users will need to manually change the latitude and longitude of the samples until they are located near the correct channel.

We wish to emphasize that the relative denudation rates do not change significantly between
495 CAIRN and reported values (as evidenced by a clustering about the 1:1 line in Figure 6). In addition previous studies contain elements modulating denudation rates that are not contained within the current version of CAIRN. For example Kirchner et al. (2001) reports true physical erosion rather than denudation and Safran et al. (2006) modified their denudation rates based on the quartz content of the source areas.

500 6.3 Comparison with the CRONUS calculators

The results from CAIRN are compared to results from both CRONUS calculators. When comparing output from the CAIRN calculator with output from the online CRONUS-2.2 calculator, far larger uncertainties (up to to 40% of the denudation rate) occur. These errors are not controlled by denudation rate (Figure 7) but are instead mainly a function of the production rate (Figure 8). In the previous
505 section, we found that errors due to spatial averaging and separation of shielding from production scaling are small. The large difference is primarily due to the difference in spallation production



rates and the over-production of muons in CRONUS version 2.2, as described by Balco et al. (2013). According to Balco et al., future versions of this CRONUS calculator will be updated to have significantly reduced muogenic production consistent with recent studies (Braucher et al., 2003; Phillips et al., 2016a; Braucher et al., 2011, 2013).

The other CRONUS calculator, CRONUScalc, incorporates new spallation production rates and muon production is calculated using production rates based on a deep core from Antarctica (Marrero et al., 2016; Phillips et al., 2016a). In order to examine the underlying source of discrepancies between the three calculators, we plot the total and muon production rates for the CAIRN, CRONUS-2.2, and CRONUScalc calculators in Figure (9). The production rates for CRONUS-2.2 are calculated directly from the MATLAB scripts available online. The CRONUScalc production rates are approximated as a three exponential analytical function with parameters shown in Table 4. Although total production rates appear relatively similar, CRONUScalc and CAIRN predict significantly smaller muon contributions than CRONUS-2.2. The result is that for the same denudation rate, the CRONUS-2.2 calculator produces significantly more (in some case 40% more) atoms than using CAIRN or CRONUScalc (Figure 10). This discrepancy between muon production is important because rapidly eroding samples accumulate a significant proportion of their nuclide concentrations below 100 g cm^{-2} , leading to a large discrepancy in calculated denudation rates between CRONUS-2.2 and the other two calculators (CAIRN and CRONUScalc), which both incorporate more recent muon models. The CAIRN outputs of topographic shielding, as well as the spatial averaging of both production scaling and shielding, are independent of these calculators and will still provide spatial averaging for use with future calculator versions, even as production rates and mechanisms are updated.

We have used the spatially averaged shielding and scaling outputs from CAIRN to determine errors between CAIRN and CRONUScalc. We find that there is a 2.5% to 5% error between the denudation rates predicted by CAIRN and those predicted by CRONUScalc (Figure 11). Currently CRONUScalc is not able to calculate very high denudation rates (for rates greater than $\sim 0.06 \text{ g cm}^{-2} \text{ yr}^{-1}$ the current version of CRONUScalc crashes; it was designed for exposure ages and becomes computationally unstable at high erosion rates) so we cannot compare CAIRN to CRONUScalc for all of the example datasets. The errors in Figure (11) arise from two sources: first, we must pass the product of the scaling (S_{effp}) and shielding ($S_{CRshield}$) to CRONUScalc rather than calculating pixel by pixel values. Second, the default muon production in CAIRN is derived from the Braucher et al. (2009) scheme, which is slightly different than the production schemes derived from Marrero et al. (2016) and Phillips et al. (2016a) (see Figure 9). In CAIRN, users can choose the muon production scheme, and we have implemented an approximation of the muon production scheme from Marrero et al. (2016) that uses the exponential form of Eq. 2 (see Table 4). It is important to note that the CAIRN implementation of muons from Marrero et al. (2016) assumes that $\Lambda = 160 \text{ g cm}^{-2}$ for spallation, whereas in CRONUScalc this attenuation length can vary as a function of latitude and



pressure. We compare the denudation rates from CAIRN using the production parameters in Table 4
545 ($\epsilon_{CAIRN-CRC}$) with the default production scheme of Braucher et al. (2009) in Figure (12). The
errors here are smaller (mostly less than 2%) suggesting that much of the error seen in Figure (11)
is due to spatial averaging.

7 Conclusions

We present an automated, open-source method for calculating catchment-averaged denudation rates
550 based on the concentrations of *in-situ* CRNs collected in stream sediment. Our catchment-averaged
denudation rate method (CAIRN) predicts CRN concentrations based on pixel-by-pixel scaling and
shielding. These concentrations are then averaged to predict the catchment-averaged concentration.
Newton iteration is later used to find the denudation rate for which the predicted concentration
matches the measured concentration and to derive associated uncertainties. In addition, CAIRN pro-
555 vides spatially averaged shielding and scaling values that can be used by other popular calculators
(which do not provide spatial averaging, e.g. CRONUS and COSMOCALC). The CAIRN method
is provided as open-source software so that reported denudation rates can be easily reproduced.

The CAIRN method is intended to streamline the computation and reporting of catchment-averaged
denudation rates, but it has limitations that may be the subject of future developments. At the mo-
560 ment CAIRN assumes steady erosion; there is no facility for incorporating transient erosion rates
which might affect nuclide concentrations in transient landscapes (e.g., Willenbring et al., 2013b;
Mudd, 2016). In addition, the method does not include a facility for nesting basins in which the
denudation rate in a large basin incorporates the denudation rates from smaller basins that it con-
tains. The calculator cannot account for differing source areas of material, so at the moment it is
565 not capable of using differencing particle size fractions to identify denudation hot spots (e.g., Riebe
et al., 2015; Carretier et al., 2016). Despite these limitations, the CAIRN method addresses the need
to provide transparent, reproducible estimates of denudation rates.

Our open source framework allows other users to update the algorithms (e.g., a nesting function
could be built on top of the current CAIRN architecture) and different atmospheric reanalysis data
570 or new muon scaling schemes can be added as needed in the future. Thus we hope it will provide a
platform for more nuanced estimates of denudation rates from cosmogenic nuclides in the future.

Software and data availability

The software is available at the LSDTopoTools Github website (<https://github.com/LSDtopotools/>).
The data files containing formatted cosmogenic data, parameter values and results, and scripts for
575 plotting figures used in this paper are also located on the Github site. All DEMs used in the analysis
were derived from Shuttle Radar Topography Mission 3 arc second data available from the United
States Geological Survey digital globe website (<http://earthexplorer.usgs.gov/>).



Author contributions

S.M. Mudd (SMM), MDH and SWDG wrote the software. MAH, SMM and S.M. Marrero analyzed
580 the data. SMM wrote the paper with contributions from other authors.

Acknowledgements. SMM and MAH are funded by U.S. Army Research Office contract number W911NF-13-
1-0478 and SMM and SWDG are funded by NERC grant NE/J009970/1. S.M. Marrero is funded by NERC
grant NE/I025840/1. This paper is published with the permission of the Executive Director of the British Geo-
logical Survey (NERC), and was supported by the Climate and Landscape Change research programme at the
585 BGS.



References

- Abbühl, L. M., Norton, K. P., Schlunegger, F., Kracht, O., Aldahan, A., and Possnert, G.: El Niño forcing on 10Be-based surface denudation rates in the northwestern Peruvian Andes?, *Geomorphology*, 123, 257–268, doi:10.1016/j.geomorph.2010.07.017, 2010.
- 590 Balco, G., Stone, J. O., Lifton, N. A., and Dunai, T. J.: A complete and easily accessible means of calculating surface exposure ages or erosion rates from 10Be and 26Al measurements, *Quaternary Geochronology*, 3, 174–195, doi:10.1016/j.quageo.2007.12.001, 2008.
- Balco, G., Soreghan, G. S., Sweet, D. E., Marra, K. R., and Bierman, P. R.: Cosmogenic-nuclide burial ages for Pleistocene sedimentary fill in Unaweep Canyon, Colorado, USA, *Quaternary Geochronology*, 18, 149–157, doi:10.1016/j.quageo.2013.02.002, 2013.
- 595 Belmont, P., Pazzaglia, F. J., and Gosse, J. C.: Cosmogenic 10Be as a tracer for hillslope and channel sediment dynamics in the Clearwater River, western Washington State, *Earth and Planetary Science Letters*, 264, 123–135, doi:10.1016/j.epsl.2007.09.013, 2007.
- Bierman, P. and Steig, E. J.: Estimating Rates of Denudation Using Cosmogenic Isotope Abundances in Sediment, *Earth Surface Processes and Landforms*, 21, 125–139, doi:10.1002/(SICI)1096-9837(199602)21:2<125::AID-ESP511>3.0.CO;2-8, 1996.
- 600 Bierman, P. R., Reuter, J. M., Pavich, M., Gellis, A. C., Caffee, M. W., and Larsen, J.: Using cosmogenic nuclides to contrast rates of erosion and sediment yield in a semi-arid, arroyo-dominated landscape, Rio Puerco Basin, New Mexico, *Earth Surface Processes and Landforms*, 30, 935–953, doi:10.1002/esp.1255, 2005.
- 605 Borchers, B., Marrero, S., Balco, G., Caffee, M., Goehring, B., Lifton, N., Nishiizumi, K., Phillips, F., Schaefer, J., and Stone, J.: Geological calibration of spallation production rates in the CRONUS-Earth project, *Quaternary Geochronology*, 31, 188–198, doi:10.1016/j.quageo.2015.01.009, 2016.
- Braucher, R., Brown, E. T., Bourlès, D. L., and Colin, F.: In situ produced 10Be measurements at great depths: implications for production rates by fast muons, *Earth and Planetary Science Letters*, 211, 251–258, doi:10.1016/S0012-821X(03)00205-X, 2003.
- 610 Braucher, R., Del Castillo, P., Siame, L., Hidy, A. J., and Bourlés, D. L.: Determination of both exposure time and denudation rate from an in situ-produced 10Be depth profile: A mathematical proof of uniqueness. Model sensitivity and applications to natural cases, *Quaternary Geochronology*, 4, 56–67, doi:10.1016/j.quageo.2008.06.001, 2009.
- 615 Braucher, R., Merchel, S., Borgomano, J., and Bourlès, D. L.: Production of cosmogenic radionuclides at great depth: A multi element approach, *Earth and Planetary Science Letters*, 309, 1–9, doi:10.1016/j.epsl.2011.06.036, 2011.
- Braucher, R., Bourlès, D., Merchel, S., Vidal Romani, J., Fernandez-Mosquera, D., Marti, K., Léanni, L., Chauvet, F., Arnold, M., Aumaitre, G., and Keddadouche, K.: Determination of muon attenuation lengths in depth profiles from in situ produced cosmogenic nuclides, *Nuclear Instruments and Methods in Physics Research Section B: Beam Interactions with Materials and Atoms*, 294, 484–490, doi:10.1016/j.nimb.2012.05.023, 2013.
- 620



- 625 Brown, E. T., Stallard, R. F., Larsen, M. C., Raisbeck, G. M., and Yiou, F.: Denudation rates determined from the accumulation of in situ-produced ^{10}Be in the luquillo experimental forest, Puerto Rico, *Earth and Planetary Science Letters*, 129, 193–202, doi:10.1016/0012-821X(94)00249-X, 1995.
- Carretier, S., Martinod, P., Reich, M., and Godderis, Y.: Modelling sediment clasts transport during landscape evolution, *Earth Surface Dynamics*, 4, 237–251, doi:10.5194/esurf-4-237-2016, 2016.
- 630 Chmeleff, J., von Blanckenburg, F., Kossert, K., and Jakob, D.: Determination of the ^{10}Be half-life by multi-collector ICP-MS and liquid scintillation counting, *Nuclear Instruments and Methods in Physics Research Section B: Beam Interactions with Materials and Atoms*, 268, 192–199, doi:10.1016/j.nimb.2009.09.012, 2010.
- Codilean, A. T.: Calculation of the cosmogenic nuclide production topographic shielding scaling factor for large areas using DEMs, *Earth Surface Processes and Landforms*, 31, 785–794, doi:10.1002/esp.1336, 2006.
- 635 Compo, G. P., Whitaker, J. S., Sardeshmukh, P. D., Matsui, N., Allan, R. J., Yin, X., Gleason, B. E., Vose, R. S., Rutledge, G., Bessemoulin, P., Brönnimann, S., Brunet, M., Crouthamel, R. I., Grant, A. N., Groisman, P. Y., Jones, P. D., Kruk, M. C., Kruger, A. C., Marshall, G. J., Mauerer, M., Mok, H. Y., Nordli, ., Ross, T. F., Trigo, R. M., Wang, X. L., Woodruff, S. D., and Worley, S. J.: The Twentieth Century Reanalysis Project, *Quarterly Journal of the Royal Meteorological Society*, 137, 1–28, doi:10.1002/qj.776, 2011.
- 640 Delunel, R., Bourlès, D. L., van der Beek, P. A., Schlunegger, F., Leya, I., Masarik, J., and Paquet, E.: Snow shielding factors for cosmogenic nuclide dating inferred from long-term neutron detector monitoring, *Quaternary Geochronology*, 24, 16–26, doi:10.1016/j.quageo.2014.07.003, 2014.
- Desilets, D. and Zreda, M.: Spatial and temporal distribution of secondary cosmic-ray nucleon intensities and applications to in situ cosmogenic dating, *Earth and Planetary Science Letters*, 206, 21–42, doi:10.1016/S0012-821X(02)01088-9, 2003.
- 645 Dethier, D. P., Ouimet, W., Bierman, P. R., Rood, D. H., and Balco, G.: Basins and bedrock: Spatial variation in ^{10}Be erosion rates and increasing relief in the southern Rocky Mountains, USA, *Geology*, 42, 167–170, doi:10.1130/G34922.1, 2014.
- DiBiase, R. A., Whipple, K. X., Heimsath, A. M., and Ouimet, W. B.: Landscape form and millennial erosion rates in the San Gabriel Mountains, CA, *Earth and Planetary Science Letters*, 289, 134–144, doi:10.1016/j.epsl.2009.10.036, 2010.
- Dunai, T.: Influence of secular variation of the geomagnetic field on production rates of in situ produced cosmogenic nuclides, *Earth and Planetary Science Letters*, 193, 197–212, <http://www.sciencedirect.com/science/article/pii/S0012821X01005039>, 2001.
- 655 Dunai, T. J.: Scaling factors for production rates of in situ produced cosmogenic nuclides: a critical reevaluation, *Earth and Planetary Science Letters*, 176, 157–169, doi:10.1016/S0012-821X(99)00310-6, 2000.
- Dunai, T. J.: *Cosmogenic Nuclides: Principles, Concepts and Applications in the Earth Surface Sciences*, Cambridge University Press, 2010.
- Dunne, J., Elmore, D., and Muzikar, P.: Scaling factors for the rates of production of cosmogenic nuclides for geometric shielding and attenuation at depth on sloped surfaces, *Geomorphology*, 27, 3–11, doi:10.1016/S0169-555X(98)00086-5, 1999.
- 660 Gosse, J. C. and Phillips, F. M.: Terrestrial in situ cosmogenic nuclides: theory and application, *Quaternary Science Reviews*, 20, 1475–1560, doi:10.1016/S0277-3791(00)00171-2, 2001.



- Granger, D. E. and Schaller, M.: Cosmogenic Nuclides and Erosion at the Watershed Scale, *Elements*, 10, 369–373, doi:10.2113/gselements.10.5.369, 2014.
- Granger, D. E. and Smith, A. L.: Dating buried sediments using radioactive decay and muogenic production of ^{26}Al and ^{10}Be , *Nuclear Instruments and Methods in Physics Research Section B: Beam Interactions with Materials and Atoms*, 172, 822–826, doi:10.1016/S0168-583X(00)00087-2, 2000.
- Granger, D. E., Kirchner, J. W., and Finkel, R.: Spatially Averaged Long-Term Erosion Rates Measured from in Situ-Produced Cosmogenic Nuclides in Alluvial Sediment, *Journal of Geology*, 104, 249–257, doi:10.1086/629823, 1996.
- Granger, D. E., Lifton, N. A., and Willenbring, J. K.: A cosmic trip: 25 years of cosmogenic nuclides in geology, *Geological Society of America Bulletin*, p. B30774.1, doi:10.1130/B30774.1, <http://gsabulletin.gsapubs.org/content/early/2013/07/23/B30774.1>, 2013.
- Guzzetti, F., Ardizzone, F., Cardinali, M., Rossi, M., and Valigi, D.: Landslide volumes and landslide mobilization rates in Umbria, central Italy, *Earth and Planetary Science Letters*, 279, 222–229, doi:10.1016/j.epsl.2009.01.005, 2009.
- Heisinger, B., Lal, D., Jull, A. J. T., Kubik, P., Ivy-Ochs, S., Knie, K., and Nolte, E.: Production of selected cosmogenic radionuclides by muons: 2. Capture of negative muons, *Earth and Planetary Science Letters*, 200, 357–369, doi:10.1016/S0012-821X(02)00641-6, 2002a.
- Heisinger, B., Lal, D., Jull, A. J. T., Kubik, P., Ivy-Ochs, S., Neumaier, S., Knie, K., Lazarev, V., and Nolte, E.: Production of selected cosmogenic radionuclides by muons: 1. Fast muons, *Earth and Planetary Science Letters*, 200, 345–355, doi:10.1016/S0012-821X(02)00640-4, 2002b.
- Hovius, N., Stark, C. P., and Allen, P. A.: Sediment flux from a mountain belt derived by landslide mapping, *Geology*, 25, 231–234, doi:10.1130/0091-7613(1997)025<0231:SFFAMB>2.3.CO;2, 1997.
- Hurst, M. D., Mudd, S. M., Walcott, R., Attal, M., and Yoo, K.: Using hilltop curvature to derive the spatial distribution of erosion rates, *Journal of Geophysical Research: Earth Surface*, 117, F02017, doi:10.1029/2011JF002057, 2012.
- Kelly, M. A., Lowell, T. V., Applegate, P. J., Phillips, F. M., Schaefer, J. M., Smith, C. A., Kim, H., Leonard, K. C., and Hudson, A. M.: A locally calibrated, late glacial ^{10}Be production rate from a low-latitude, high-altitude site in the Peruvian Andes, *Quaternary Geochronology*, doi:10.1016/j.quageo.2013.10.007, 2015.
- Kirchner, J. W., Finkel, R. C., Riebe, C. S., Granger, D. E., Clayton, J. L., King, J. G., and Megahan, W. F.: Mountain erosion over 10 yr, 10 k.y., and 10 m.y. time scales, *Geology*, 29, 591–594, doi:10.1130/0091-7613(2001)029<0591:MEOYKY>2.0.CO;2, 2001.
- Korschinek, G., Bergmaier, A., Faestermann, T., Gerstmann, U. C., Knie, K., Rugel, G., Wallner, A., Dillmann, I., Dollinger, G., von Gostomski, C. L., Kossert, K., Maiti, M., Poutivtsev, M., and Remmert, A.: A new value for the half-life of ^{10}Be by Heavy-Ion Elastic Recoil Detection and liquid scintillation counting, *Nuclear Instruments and Methods in Physics Research Section B: Beam Interactions with Materials and Atoms*, 268, 187–191, doi:10.1016/j.nimb.2009.09.020, 2010.
- Korup, O.: Distribution of landslides in southwest New Zealand, *Landslides*, 2, 43–51, doi:10.1007/s10346-004-0042-0, 2005.
- Lal, D.: Cosmic ray labeling of erosion surfaces: in situ nuclide production rates and erosion models, *Earth and Planetary Science Letters*, 104, 424–439, doi:10.1016/0012-821X(91)90220-C, 1991.



- 705 Lifton, N., Sato, T., and Dunai, T. J.: Scaling in situ cosmogenic nuclide production rates using analytical approximations to atmospheric cosmic-ray fluxes, *Earth and Planetary Science Letters*, 386, 149–160, doi:10.1016/j.epsl.2013.10.052, 2014.
- Lifton, N. A., Bieber, J. W., Clem, J. M., Duldig, M. L., Evenson, P., Humble, J. E., and Pyle, R.: Addressing solar modulation and long-term uncertainties in scaling secondary cosmic rays for in situ cosmogenic nuclide applications, *Earth and Planetary Science Letters*, 239, 140–161, doi:10.1016/j.epsl.2005.07.001, 2005.
- 710 Lupker, M., Blard, P.-H., Lavé, J., France-Lanord, C., Leanni, L., Puchol, N., Charreau, J., and Bourlès, D.: ¹⁰Be-derived Himalayan denudation rates and sediment budgets in the Ganga basin, *Earth and Planetary Science Letters*, 333–334, 146–156, doi:10.1016/j.epsl.2012.04.020, 2012.
- Marrero, S. M., Phillips, F. M., Borchers, B., Lifton, N., Aumer, R., and Balco, G.: Cosmogenic nuclide systematics and the CRONUScal program, *Quaternary Geochronology*, 31, 160–187, doi:10.1016/j.quageo.2015.09.005, 2016.
- 715 Mudd, S. M.: Detection of transience in eroding landscapes, *Earth Surface Processes and Landforms*, pp. n/a–n/a, doi:10.1002/esp.3923, <http://onlinelibrary.wiley.com/doi/10.1002/esp.3923/abstract>, 2016.
- Munack, H., Korup, O., Resentini, A., Limonta, M., Garzanti, E., Blöthe, J. H., Scherler, D., Wittmann, H., and Kubik, P. W.: Postglacial denudation of western Tibetan Plateau margin outpaced by long-term exhumation, *Geological Society of America Bulletin*, p. B30979.1, doi:10.1130/B30979.1, 2014.
- 720 Muzikar, P.: General models for episodic surface denudation and its measurement by cosmogenic nuclides, *Quaternary Geochronology*, 4, 50–55, doi:10.1016/j.quageo.2008.06.004, 2009.
- Niemi, N. A., Oskin, M., Burbank, D. W., Heimsath, A. M., and Gabet, E. J.: Effects of bedrock landslides on cosmogenically determined erosion rates, *Earth and Planetary Science Letters*, 237, 480–498, doi:10.1016/j.epsl.2005.07.009, 2005.
- 725 Nishiizumi, K.: Preparation of ²⁶Al AMS standards, *Nuclear Instruments and Methods in Physics Research Section B: Beam Interactions with Materials and Atoms*, 223–224, 388–392, doi:10.1016/j.nimb.2004.04.075, 2004.
- Norton, K. P. and Vanacker, V.: Effects of terrain smoothing on topographic shielding correction factors for cosmogenic nuclide-derived estimates of basin-averaged denudation rates, *Earth Surface Processes and Landforms*, 34, 145–154, doi:10.1002/esp.1700, 2009.
- 730 Ouimet, W. B., Whipple, K. X., and Granger, D. E.: Beyond threshold hillslopes: Channel adjustment to base-level fall in tectonically active mountain ranges, *Geology*, 37, 579–582, doi:10.1130/G30013A.1, 2009.
- Palumbo, L., Hetzel, R., Tao, M., and Li, X.: Topographic and lithologic control on catchment-wide denudation rates derived from cosmogenic ¹⁰Be in two mountain ranges at the margin of NE Tibet, *Geomorphology*, 117, 130–142, doi:10.1016/j.geomorph.2009.11.019, 2010.
- 735 Palumbo, L., Hetzel, R., Tao, M., and Li, X.: Catchment-wide denudation rates at the margin of NE Tibet from in situ-produced cosmogenic ¹⁰Be, *Terra Nova*, 23, 42–48, doi:10.1111/j.1365-3121.2010.00982.x, 2011.
- Parker, G. and Perg, L. A.: Probabilistic formulation of conservation of cosmogenic nuclides: effect of surface elevation fluctuations on approach to steady state, *Earth Surface Processes and Landforms*, 30, 1127–1144, doi:10.1002/esp.1266, 2005.
- 740 Phillips, F. M., Argento, D. C., Balco, G., Caffee, M. W., Clem, J., Dunai, T. J., Finkel, R., Goehring, B., Gosse, J. C., Hudson, A. M., Jull, T. A., Kelly, M., Kurz, M., Lal, D., Lifton, N., Marrero, S. M., Nishiizumi, K.,



- Reedy, R., Schaefer, J., Stone, J. O., Swanson, T., and Zreda, M. G.: The CRONUS-Earth project: a synthesis,
745 Quaternary Geochronology, 31, 119–154, doi:10.1016/j.quageo.2015.09.006, 2016a.
- Phillips, F. M., Kelly, M. A., Hudson, A. M., Stone, J. O., Schaefer, J., Marrero, S. M., Fifield, L. K., Finkel,
R., and Lowell, T.: CRONUS-Earth calibration samples from the Huancané II moraines, Quelccaya Ice Cap,
Peru, Quaternary Geochronology, 31, 220–236, doi:10.1016/j.quageo.2015.10.005, 2016b.
- Portenga, E. W. and Bierman, P. R.: Understanding Earth's eroding surface with ^{10}Be , GSA Today, 21, 4–10,
750 doi:10.1130/G111A.1, 2011.
- Riebe, C. S., Sklar, L. S., Lukens, C. E., and Shuster, D. L.: Climate and topography control the size and
flux of sediment produced on steep mountain slopes, Proceedings of the National Academy of Sciences, p.
201503567, doi:10.1073/pnas.1503567112, 2015.
- Safran, E. B., Blythe, A., and Dunne, T.: Spatially Variable Exhumation Rates in Orogenic Belts: An Andean
755 Example, Journal of Geology, 114, 665–681, doi:10.1086/507613, 2006.
- Schaller, M. and Ehlers, T. A.: Limits to quantifying climate driven changes in denudation rates with cos-
mogenic radionuclides, Earth and Planetary Science Letters, 248, 153–167, doi:10.1016/j.epsl.2006.05.027,
2006.
- Schaller, M., Ehlers, T. A., Blum, J. D., and Kallenberg, M. A.: Quantifying glacial moraine age, denudation,
760 and soil mixing with cosmogenic nuclide depth profiles, Journal of Geophysical Research: Earth Surface,
114, F01 012, doi:10.1029/2007JF000921, 2009.
- Scherler, D., Bookhagen, B., and Strecker, M. R.: Tectonic control on ^{10}Be -derived erosion rates in
the Garhwal Himalaya, India, Journal of Geophysical Research: Earth Surface, 119, 2013JF002 955,
doi:10.1002/2013JF002955, 2014.
- 765 Schildgen, T. F., Phillips, W. M., and Purves, R. S.: Simulation of snow shielding corrections for cosmogenic
nuclide surface exposure studies, Geomorphology, 64, 67–85, 2005.
- Stone, J. O.: Air pressure and cosmogenic isotope production, Journal of Geophysical Research, 105, 23 753,
doi:10.1029/2000JB900181, 2000.
- Uppala, S. M., Källberg, P., Simmons, A., Andrae, U., Bechtold, V. d., Fiorino, M., Gibson, J., Haseler, J.,
770 Hernandez, A., Kelly, G., et al.: The ERA-40 re-analysis, Quarterly Journal of the Royal Meteorological
Society, 131, 2961–3012, 2005.
- Vermeesch, P.: CosmoCalc: An Excel add-in for cosmogenic nuclide calculations, Geochemistry, Geophysics,
Geosystems, 8, Q08 003, doi:10.1029/2006GC001530, 2007.
- von Blanckenburg, F. and Willenbring, J. K.: Cosmogenic Nuclides: Dates and Rates of Earth-Surface Change,
775 Elements, 10, 341–346, doi:10.2113/gselements.10.5.341, [http://elements.geoscienceworld.org/content/10/
5/341](http://elements.geoscienceworld.org/content/10/5/341), 2014.
- West, A. J., Hetzel, R., Li, G., Jin, Z., Zhang, F., Hilton, R. G., and Densmore, A. L.: Dilution of ^{10}Be in
detrital quartz by earthquake-induced landslides: Implications for determining denudation rates and potential
to provide insights into landslide sediment dynamics, Earth and Planetary Science Letters, 396, 143–153,
780 doi:10.1016/j.epsl.2014.03.058, 2014.
- West, A. J., Arnold, M., Aumaître, G., Bourlès, D. L., Keddadouche, K., Bickle, M., and Ojha, T.: High natural
erosion rates are the backdrop for present-day soil erosion in the agricultural Middle Hills of Nepal, Earth
Surface Dynamics, 3, 363–387, doi:10.5194/esurf-3-363-2015, 2015.



- Willenbring, J. K., Codilean, A. T., and McElroy, B.: Earth is (mostly) flat: Apportionment of the flux of
785 continental sediment over millennial time scales, *Geology*, p. G33918.1, doi:10.1130/G33918.1, 2013a.
- Willenbring, J. K., Gasparini, N. M., Crosby, B. T., and Brocard, G.: What does a mean mean? The tem-
poral evolution of detrital cosmogenic denudation rates in a transient landscape, *Geology*, 41, 1215–1218,
doi:10.1130/G34746.1, 2013b.
- Yanites, B. J., Tucker, G. E., and Anderson, R. S.: Numerical and analytical models of cosmogenic radionuclide
790 dynamics in landslide-dominated drainage basins, *Journal of Geophysical Research (Earth Surface)*, 114,
F01 007, doi:10.1029/2008JF001088, 2009.
- Zweck, C., Zreda, M., and Desilets, D.: Snow shielding factors for cosmogenic nuclide dating inferred
from Monte Carlo neutron transport simulations, *Earth and Planetary Science Letters*, 379, 64–71,
doi:10.1016/j.epsl.2013.07.023, 2013.



Table 1. Absolute maximum residuals (i.e., greatest residual within the DEM) for different combinations of $\Delta\theta$ and $\Delta\phi$ used in shielding calculations for a high relief basin in the Himalayas.

$\Delta\phi$, degrees	$\Delta\theta$, degrees									
	1	2	3	5	8	10	15	30	45	60
1	0.000	0.002	0.004	0.009	0.010	0.011	0.027	0.053	0.063	0.081
2	0.004	0.004	0.005	0.009	0.010	0.012	0.029	0.057	0.064	0.080
3	0.008	0.008	0.008	0.010	0.011	0.012	0.027	0.053	0.062	0.081
5	0.014	0.015	0.016	0.017	0.018	0.018	0.030	0.056	0.065	0.087
8	0.023	0.023	0.026	0.025	0.027	0.030	0.039	0.064	0.082	0.093
10	0.036	0.037	0.033	0.040	0.035	0.040	0.037	0.063	0.074	0.104
15	0.057	0.059	0.058	0.060	0.060	0.058	0.065	0.084	0.100	0.122
20	0.072	0.071	0.073	0.075	0.077	0.076	0.083	0.111	0.109	0.138
30	0.171	0.172	0.168	0.176	0.167	0.167	0.173	0.188	0.160	0.242
45	0.337	0.340	0.332	0.335	0.346	0.335	0.332	0.393	0.385	0.430
60	0.352	0.352	0.352	0.352	0.352	0.352	0.352	0.352	0.385	0.418



Table 2. Datasets used for method comparisons. ^{10}Be production rate (Prod rate) is given for sea level, high latitude and in units of atoms $\text{g}^{-1} \text{yr}^{-1}$. 'CR' or 'CR muons' refers to the spallation or muon calculation methods and production rates used in CRONUS-2.2 (Balco et al., 2008). The scaling values, production rates, topographic shielding and notes reported in this table are for the original studies: CAIRN uses the same settings (see Table (3) for its calculations regardless of site location.

Study	Location	Scaling	Prod rate	Topo Shielding	Other Notes
Bierman et al. (2005)	New Mexico, USA	Lal/Stone	5.2	None.	$\rho = 2.7 \text{ g cm}^{-3}$, no muons.
Dethier et al. (2014)	Colorado, USA	Lal/Stone	4.49 (CR)	None.	$\rho = 2.7 \text{ g cm}^{-3}$, fast muons only.
Kirchner et al. (2001)	Idaho, USA	Lal/Stone	4.72	Dunne et al. (1999), details not given.	Corrections for chemical weathering.
Munack et al. (2014)	Ladakh, India	Lal magnetic	4.49 (CR)	Pixel-by-pixel, but details not given.	CR muons. Snow and ice shielding considered.
Palumbo et al. (2010) and Palumbo et al. (2011)	Tibet	Dunai (2000)	5.12	Codilean (2006), $\Delta\phi$, $\Delta\theta$ not reported.	Muons using Granger and Smith (2000) scheme. $\rho = 2.65 \text{ g cm}^{-3}$.
Safran et al. (2006)	Bolivia	Dunai (2000)	None.	No muons. ρ not reported. Corrections for quartz fraction.	
Scherler et al. (2014)	Garwahl Himalaya	Lal magnetic	4.49 (CR)	Pixel-by-pixel, but details not given.	CR muons. Snow and ice shielding considered.

Table 3. Default parameters used in the CAIRN model.

Parameter	Value	Source
$\lambda_{^{10}\text{Be}}$	$500 \cdot 10^{-9} \text{ yr}^{-1}$	Chmeleff et al. (2010); Korschinek et al. (2010)
$\lambda_{^{26}\text{Al}}$	$980 \cdot 10^{-9} \text{ yr}^{-1}$	Nishiizumi (2004)
Λ_i	160;1500;4320 g cm^{-2}	From COSMOCALC version 2.0 to mimic Braucher et al. (2009)
$^{10}\text{Be } P_{SLHL}$	4.30 atoms $\text{g}^{-1} \text{yr}^{-1}$	From COSMOCALC version 2.0 to mimic Braucher et al. (2009)
$^{10}\text{Be } F_i$	0.9887; 0.0027; 0.0086 (dimensionless)	From COSMOCALC version 2.0 to mimic Braucher et al. (2009)
$^{26}\text{Al } P_{SLHL}$	31.10 atoms $\text{g}^{-1} \text{yr}^{-1}$	From COSMOCALC version 2.0
$^{26}\text{Al } F_i$	0.9699; 0.00275; 0.0026 (dimensionless)	From COSMOCALC version 2.0 to mimic Braucher et al. (2009)



Table 4. Parameters used for production of ^{10}Be which approximate the scheme in CRONUScalc (Marrero et al., 2016). $\lambda_{^{10}\text{Be}}$ values are the same as defaults listed previously. The F_i values represent spallation and fast and slow muons, respectively.

Parameter	Value
Λ_i	160;1460;11040 g cm^{-2}
$^{10}\text{Be } P_{SLHL}$	4.075 $\text{atoms g}^{-1} \text{yr}^{-1}$
$^{10}\text{Be } F_i$	0.9837; 0.0137; 0.0025 (dimensionless.)

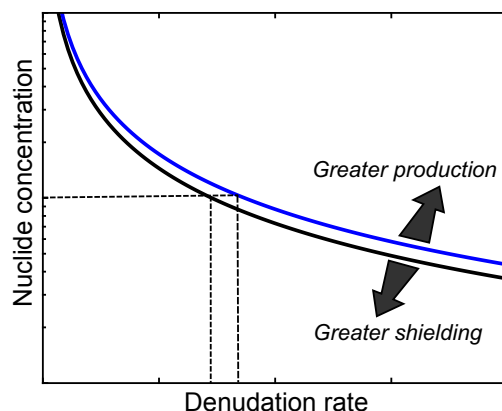


Figure 1. A schematic drawing of the predicted concentration of a nuclide as a function of denudation rate. If production rates are assumed to be higher, the predicted concentration will be higher for a given denudation rate. If shielding is greater, the predicted concentration is lower for a predicted denudation rate. Thus assumptions about production and shielding will affect the inferred denudation rate given a sample with fixed concentration, shown with the dashed lines.

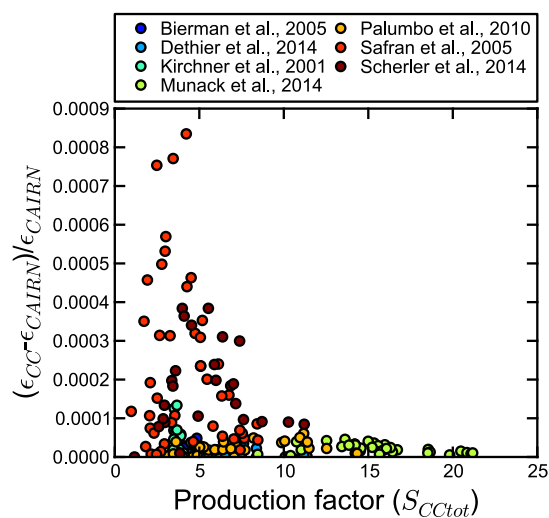


Figure 2. Errors between the denudation rate calculated by CAIRN (ϵ_{CAIRN}) and the denudation rate using the production factor (S_{CCtot}) (which includes production scaling and shielding) passed to COSMOCALC (ϵ_{CC}).

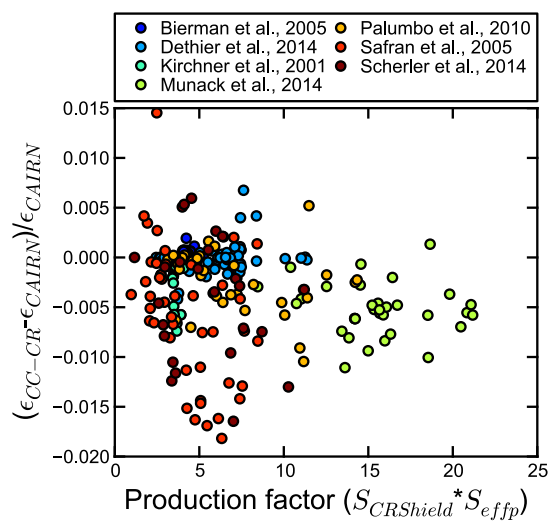


Figure 3. Errors between the denudation rate calculated by CAIRN (ϵ_{CAIRN}) and the denudation rate using separate spatial averages for shielding and production scaling that are then averaged ($\epsilon_{CC-CRONUS}$) as a function of production factor. In this case the production factor is calculated by multiplying the separately averaged shielding ($S_{CRShield}$) and scaling (S_{effp}) factors. This approach emulates the data requirements for CRONUS-2.2, which calculates production scaling and accepts a single shielding factor (for snow and topography combined). Although the shielding and scaling emulate data requirements for CRONUS-2.2, the denudation rate is calculated using the exponential production method of CAIRN and COSMOCALC.

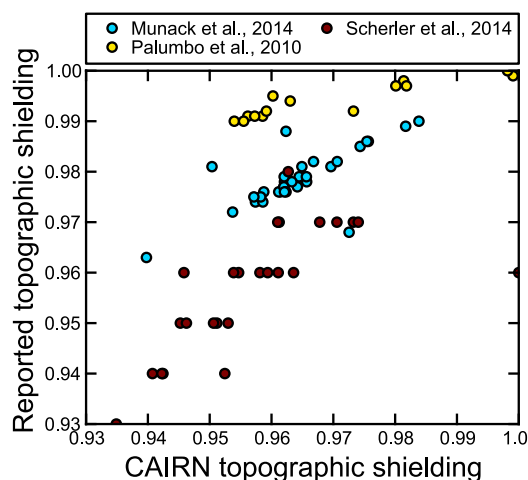


Figure 4. Topographic shielding (S_t) calculated using $\Delta\phi = 5$, $\Delta\theta = 8$ plotted as a function of reported shielding.

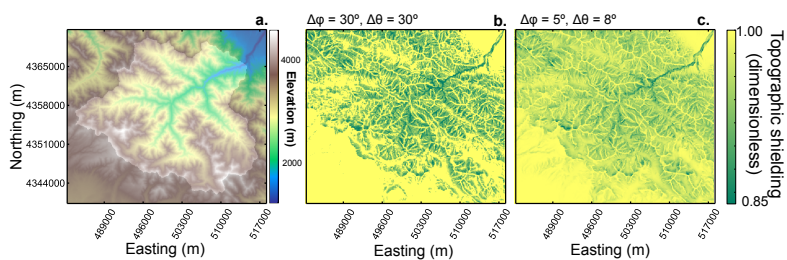


Figure 5. Comparison of the topographic shielding for different values of $\Delta\phi$ and $\Delta\theta$. The Tibetan basin is for sample 07C13 in Palumbo et al. (2011). Maps are projected into WGS1984, UTM zone 47N. The basin is shown in plot **a**, whereas the topographic shielding factor is shown in plots **b** and **c**.

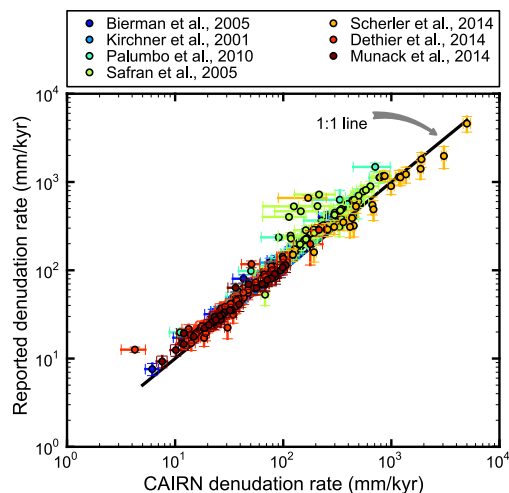


Figure 6. Comparison of denudation rates reported by selected studies plotted against denudation rates predicted by CAIRN. The denudation rates for individual studies use their original assumptions of the density of the surface material, as reported in Table 2. The results from CAIRN in this plot use a density of 2.65 g cm^{-2} .

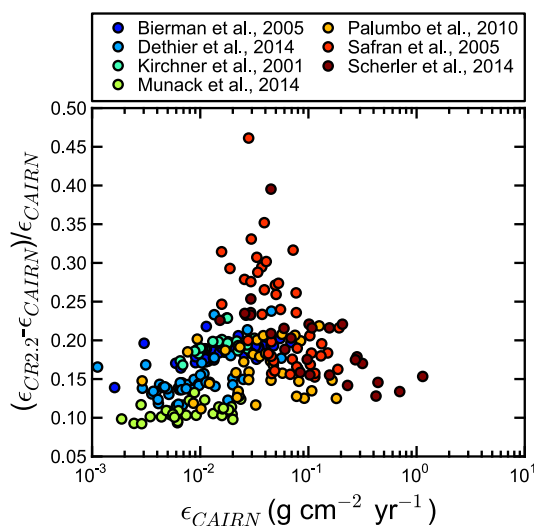


Figure 7. Errors between the denudation rate calculated by CAIRN (ϵ_{CAIRN}) and the denudation rate calculated with CRONUS-2.2 ($\epsilon_{CR2.2}$) as a function of CAIRN denudation rate.

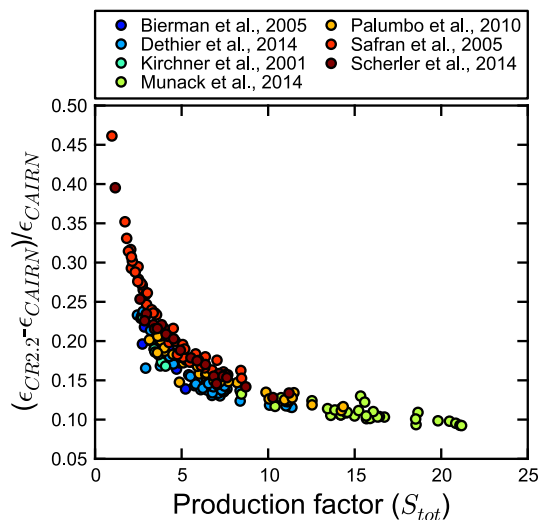


Figure 8. Errors between the denudation rate calculated by CAIRN (ϵ_{CAIRN}) and the denudation rate calculated with CRONUS-2.2 ($\epsilon_{CR2.2}$) as a function of the total scaling (S_{tot}).

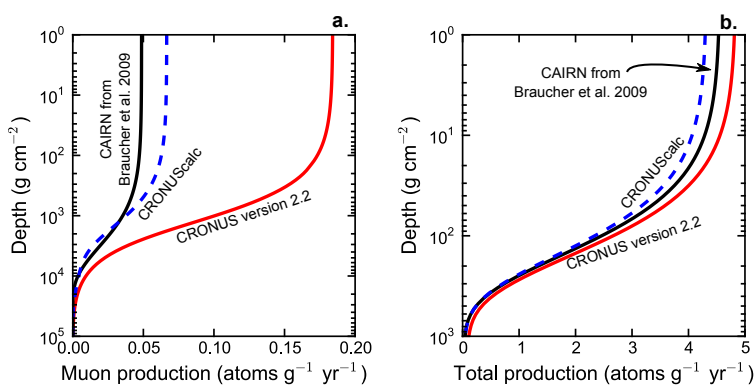


Figure 9. Production rates of ^{10}Be as a function of depth for muons only (a.) and total production (b.). These production rates are calculated using the Lal/Stone scaling at 70 degrees North and with a pressure of 1007 hPa (near sea level). Note the logarithmic depth scale: eroding particles spend a large amount of their exposure history below 100 g cm^{-2} and so increased muon production at these depths, despite being a small fraction of the total production, plays a significant role in determining the total nuclide concentration (see Figure 10).

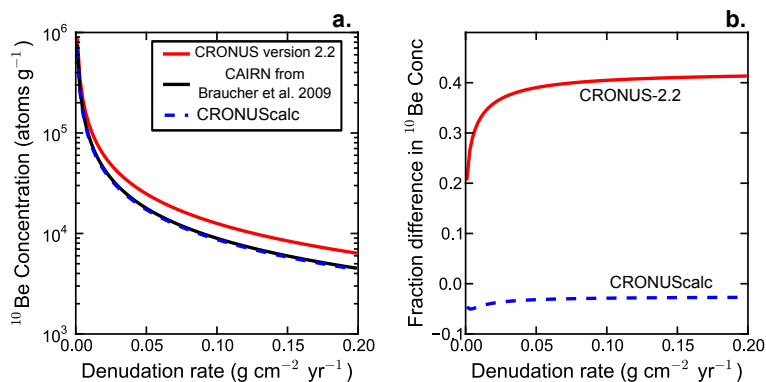


Figure 10. Concentrations as a function of denudation rate (a.) and the fractional differences between the predicted concentration from the Braucher et al. (2009) approximation used in CAIRN and both CRONUS-2.2 Balco et al. (2008) and CRONUScalc Marrero et al. (2016). These concentrations are calculated for a hypothetical site at 70 degrees North and near sea level (1007 hPa). Note that although the default production scheme in CAIRN is the Braucher et al. (2009) scheme, the production from CRONUScalc (Marrero et al., 2016) can also be used (see Table (4)).

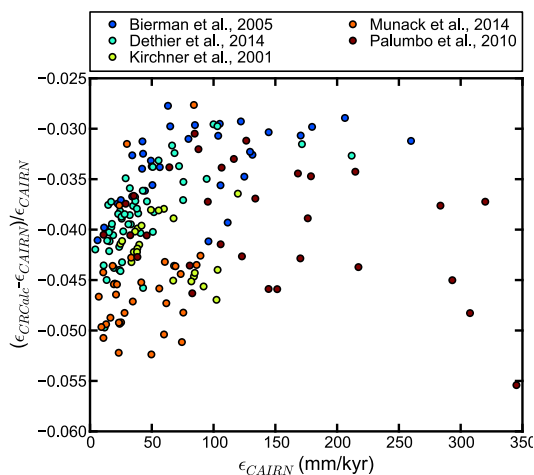


Figure 11. Errors between the denudation rate calculated by CAIRN (ϵ_{CAIRN}) and the denudation rate calculated with CRONUScalc (ϵ_{CRCalc}) as a function of CAIRN denudation rate for selected studies.

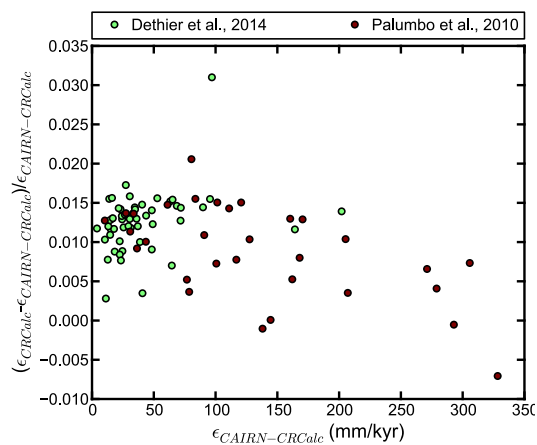


Figure 12. Errors between the denudation rate calculated by CAIRN using the parameters in Table 4 to approximate CRONUScale production ($\epsilon_{CAIRN-CRUScale}$) and the denudation rate calculated with CRONUScale ($\epsilon_{CRUScale}$) as a function of CAIRN denudation rate for selected studies.



Algorithm 1 Calculating denudation rates on a pixel-by-pixel basis

- 1: Make initial denudation rate guess based on spallation only at outlet pressure and latitude.
 - 2: **repeat**
 - 3: **for all** Pixels in basin **do**
 - 4: Calculate CRN flux based on denudation rate using Eq. 13
 - 5: **end for**
 - 6: Average the CRN concentration over the basin
 - 7: Change denudation rate by small increment
 - 8: **for all** Pixels in basin **do**
 - 9: Calculate CRN flux based on updated denudation rate using Eq. 13
 - 10: **end for**
 - 11: Calculate new denudation rate based on the change in error between calculated and measured CRN concentrations (i.e., Newton's method).
 - 12: Calculate change in effective denudation rate
 - 13: **until** Change in effective denudation rate > tolerance
-